

# Dual-Reference Design for Holographic Coherent Diffraction Imaging

David A. Barmherzig\*   Ju Sun†   Emmanuel J. Candès‡   T.J. Lane§   Po-Nan Li¶

July 28, 2022

## Abstract

A new reference design is introduced for Holographic Coherent Diffraction Imaging. This consists of two reference portions —being “block” and “pinhole” shaped regions —adjacent to the imaging specimen. Expected error analysis on data following a Poisson shot noise model shows that the dual-reference scheme produces smaller weighting of error across the frequency spectrum than does the leading single-reference schemes. Numerical experiments on simulated data also shows the dual-reference scheme achieving a smaller recovery error than the leading single-reference schemes.

## 1 Introduction

### 1.1 Holographic CDI and Holographic Phase Retrieval

Coherent Diffraction Imaging, or CDI, is a scientific imaging technique used for resolving nanoscale image specimens, such as macroviruses, proteins, and crystals [MCKS99]. In CDI, a coherent radiation source (often being an X-ray beam) is diffracted after being incident upon an imaging specimen. The resulting photon flux is then measured at a far-field detector and is approximately proportional to the squared magnitude of the Fourier transform of the electric field within the diffraction area. Determining the specimen’s electron density is then in principle possible via solving the *phase retrieval* problem, which is the mathematical inverse problem of recovering a signal from the squared magnitudes of its Fourier transform.

In a variant of this technique known as Holographic CDI, a “reference” portion of the area from which diffraction occurs—typically a simple geometric shape cut out from the metal apparatus surrounding the specimen—is a priori known from experimental design (see Fig. 1). The resulting inverse problem, in which a portion of the signal to be recovered is already known, is known as the *holographic phase retrieval* problem.

For any reference choice satisfying mild assumptions, the holographic phase retrieval problem can be solved deterministically by solving a structured linear system [BSC<sup>+</sup>19]. However, different reference choices will have different noise stability properties. It is shown in [BSC<sup>+</sup>19] that, under a Poisson shot noise model, the expected squared recovery error is given by  $\|Y\|_1 / N_p \cdot \langle S_R, Y \rangle$ , where  $Y$  is the squared Fourier transform magnitude,  $N_p$  is the nominal number of photons reaching the detector, and  $S_R$  is the *error weighting factor* which is a function of the reference  $R$  chosen (see Section 3).

For the single-reference scheme of the form  $[X, R]$ , where  $X$  is the unknown signal and  $R$  is the known reference, our previous work [BSC<sup>+</sup>19] revealed the relative merits of two popular references: the “block reference”  $R_B$  (shown in Fig. 3a) induces an  $S_{R_B}$  that weights low-frequency components of  $Y$  optimally

\*Institute for Computational and Mathematical Engineering, Stanford University, Stanford, CA 94305, U.S.A.

†Department of Mathematics, Stanford University, Stanford, CA 94305, U.S.A.

‡Department of Mathematics and Department of Statistics, Stanford University, Stanford, CA 94305, U.S.A.

§SLAC National Accelerator Laboratory, Menlo Park, CA 94025, U.S.A.

¶Department of Electrical Engineering, Stanford University, Stanford, CA 94305, U.S.A.

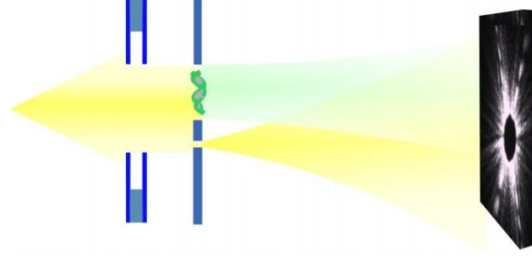


**Figure 1:** Holographic CDI schematic. The upper portion of the diffraction area contains the imaging specimen of interest, and the lower portion consists of a known “reference” shape. Image courtesy of [SLLF12].

but high-frequency components suboptimally, whereas the “pinhole reference” (shown in Fig. 3b) gives an  $S_{R_P}$  that provides smaller weighting to high-frequency components than other references (see Fig. 6). It is a natural question whether the merits of the two references can be integrated.

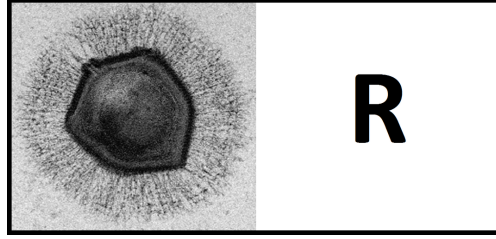


**Figure 2:** Schematic of the diffraction area in Holographic CDI containing a specimen and a known (single) reference portion.

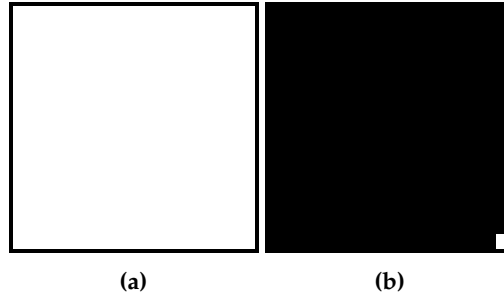


**Figure 3:** Two popular choices for the reference  $R$  shown in Fig. 2 are the block reference (Fig. 3a) and the pinhole reference (Fig. 3b). The specimen shown is the Mimivirus, courtesy of [GKL<sup>+</sup>08].

## 1.2 Our Contributions

In this paper, we show that the simple idea of augmenting the two references to the unknown specimen does the trick. Specifically, we propose a “dual-reference” design, which contains both a block and pinhole shaped region (see Fig. 4). The dual-reference gives rise to an error weighting factor  $S_{R_{B,P}}$  which provides small weighting across the whole frequency spectrum, combining the best features of both the block and pinhole references. Numerical experiments on simulated CDI data, which is subject to Poisson shot noise, consistently shows a smaller recovery error using the dual-reference than using the leading single-reference designs.

## 2 Dual-Reference Design and Recovery Algorithm

**Definition 2.1.** The block reference  $R_B \in \mathbb{R}^{n \times n}$  and the pinhole reference  $R_P \in \mathbb{R}^{n \times n}$  are defined respectively by

$$R_B(t_1, t_2) = 1, \quad t_1, t_2 \in \{0, \dots, n-1\}, \quad (2.1)$$

and

$$R_P(t_1, t_2) = \begin{cases} 1, & t_1 = t_2 = n-1 \\ 0, & \text{otherwise} \end{cases}. \quad (2.2)$$

They are shown in Fig. 3a and Fig. 3b, respectively. Suppose that  $X \in \mathbb{C}^{n \times n}$  is an “unknown” specimen. Consider  $\mathcal{X} \in \mathbb{C}^{(2n) \times (2n)}$  given by:

$$\mathcal{X} = \begin{bmatrix} X & R_B \\ R_P & \mathbf{0}_{n \times n} \end{bmatrix}, \quad (2.3)$$

where  $\mathbf{0}_{n \times n}$  is the  $n \times n$  all-zero matrix. We shall assume that the magnitudes of the entries of  $X$  are within the interval  $[0, 1]$ . By this convention, 0 values represent areas where the incoming beam is entirely blocked, and 1 values represent areas where the incoming beam passes through unimpeded—which would be “empty space”.

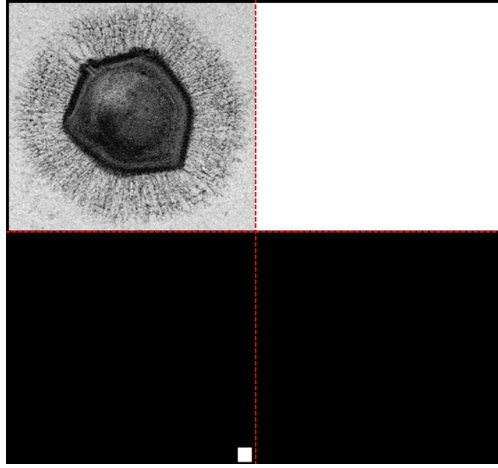


**Figure 4:** Schematic of the dual-reference. The red dotted line (added for illustration purposes) separates the four quadrants of the setup, as described by Eq. (2.3). The specimen shown is the mimivirus, courtesy of [GKL<sup>+</sup>08].

Suppose that  $m \geq 4n - 1$  and that  $Y = |\hat{\mathcal{X}}|^2 \in \mathbb{C}^{m \times m}$  are the  $m \times m$  oversampled Fourier transform magnitudes<sup>1</sup> of  $\mathcal{X}$ . We seek to recover  $X$  from  $Y^*$ , which is a possibly noise-corrupted version of  $Y$ . We propose a recovery algorithm based on solving a linear system, which is effectively the *referenced deconvolution* algorithm introduced in [BSC<sup>+</sup>19] adapted to our current reference scheme.

1. Given  $Y^*$ , apply an inverse Fourier transform ( $\mathbb{C}^{m \times m} \mapsto \mathbb{C}^{(4n-1) \times (4n-1)}$ ) to obtain  $A_{\mathcal{X}}^*$ , the noisy autocorrelation of  $\mathcal{X}$ .<sup>2</sup> This can be expressed as  $A_{\mathcal{X}}^* = \frac{1}{m^2} F^* Y^* (F^*)^T$ , where  $F \in \mathbb{C}^{m \times (4n-1)}$  is given by  $F(k, t) = e^{-2\pi i k t / m} \forall (k, t) \in \{0, \dots, m-1\} \times \{-(2n-1), \dots, 2n-1\}$ .
2. Let  $\mathcal{P}_1 = [\mathbf{0}_{n \times n}, I_n, \mathbf{0}_{n \times (2n-1)}]$  and  $\mathcal{P}_2 = [I_n, \mathbf{0}_{n \times (3n-1)}]$ . It follows that  $\mathcal{P}_1 A_{\mathcal{X}}^* \mathcal{P}_2^T \in \mathbb{R}^{n \times n}$  (resp.,  $\mathcal{P}_2 A_{\mathcal{X}}^* \mathcal{P}_1^T \in \mathbb{R}^{n \times n}$ ) is (without noise) equal to the top-left quadrant of the cross-correlation of  $X$  and  $R_B$  (resp.,  $X$  and  $R_P$ ). We thus denote this as  $C_{[X, R_B]}^{\diamond*}$  (resp.,  $C_{[X, R_P]}^{\diamond*}$ ).

<sup>1</sup>Here, the absolute value notation is understood in the pointwise sense.

<sup>2</sup>It is well-known that the inverse Fourier transform of the Fourier transform (with sufficient oversampling) magnitude squares of a signal is equal to the signal’s autocorrelation [OS09].

3. Let  $M_{R_B}$  (resp.,  $M_{R_P}$ )  $\in \mathbb{R}^{n^2 \times n^2}$  be the matrix satisfying  $M_{R_B} \text{vec}(X) = \text{vec}(C_{[X, R_B]}^\circ)$  (resp.,  $M_{R_B} \text{vec}(X) = \text{vec}(C_{[X, R_P]}^\circ)$ ).<sup>3</sup> It follows that  $M_{R_B} = \mathbf{1}_L \otimes \mathbf{1}_L$ , where  $\mathbf{1}_L \in \mathbb{R}^{n \times n}$  is the lower-triangular matrix consisting of all ones on and below the main diagonal, and that  $M_{R_P} = I_{n^2}$ . Let  $M = [M_{R_B}; M_{R_P}]$  and  $b = [\text{vec}(C_{[X, R_B]}^\circ); \text{vec}(C_{[X, R_P]}^\circ)]$ . The signal  $X$  is estimated as the solution to the least-squares problem

$$X^* = \arg \min_{X \in \mathbb{C}^{n \times n}} \|M \text{vec}(X) - b\|^2.$$

Analytically, this is given by

$$\text{vec}(X^*) = M^\dagger b = (M^T M)^{-1} M^T b.$$

Combining these steps and the well-known matrix Kronecker product identity that  $A = BCD \iff \text{vec}(A) = (D^T \otimes B) \text{vec}(C)$ , it then follows that

$$\text{vec}(X^*) = T_{R_{B,P}} \text{vec}(Y^*), \quad (2.4)$$

where

$$T_{R_{B,P}} = \frac{1}{m^2} M^\dagger \begin{bmatrix} \mathcal{P}_2 F^* \otimes \mathcal{P}_1 F^* \\ \mathcal{P}_1 F^* \otimes \mathcal{P}_2 F^* \end{bmatrix}. \quad (2.5)$$

Note that this algorithm gives a linear relationship between  $X^*$  and  $Y^*$ . In the noiseless setting, it exactly recovers the signal  $X$ . In the noisy setting, it returns the least-squares solution to

$$\min_{X \in \mathbb{C}^{n \times n}} \|Y^* - |\hat{\mathcal{X}}|^2\|^2. \quad (2.6)$$

### 3 Analysis of the Recovery Error

For any data  $Y^*$  following a known probability distribution, it follows from Eq. (2.4) that

$$\begin{aligned} \mathbb{E} \|X^* - X\|_F^2 &= \\ \langle T_R^* T_R, \mathbb{E} [\text{vec}(Y^*) - \text{vec}(Y)] [\text{vec}(Y^*) - \text{vec}(Y)]^* \rangle, \end{aligned} \quad (3.1)$$

where  $\|\cdot\|_F^2$  denotes the Frobenius norm, and  $\langle \cdot, \cdot \rangle$  denotes the Frobenius inner product.

In CDI, detector measurements of photon flux are subject to quantum shot noise. This is due to intrinsic quantum fluctuations which cannot be removed by any measurement system. The resulting photon flux measurements follow the Poisson shot noise distribution given by

$$Y^* \sim_{\text{ind}} \frac{\|Y\|_1}{N_p} \text{Pois}\left(\frac{N_p}{\|Y\|_1} Y\right), \quad (3.2)$$

where  $N_p$  is the expected (or nominal) number of photons reaching the detector, and  $\|Y\|_1$  is understood as the  $\ell_1$  norm of a vectorized version of  $Y$  [WTT<sup>+</sup>16]. As derived in [BSC<sup>+</sup>19], it then follows from Eq. (2.4) that

$$\mathbb{E} \|X^* - X\|_F^2 = \frac{\|Y\|_1}{N_p} \langle S_{R_{B,P}}, Y \rangle, \quad (3.3)$$

where

$$S_{R_{B,P}} = \text{reshape}(\text{diag}(T_R^* T_R), m, m), \quad (3.4)$$

and  $\text{reshape}(\cdot, m, m)$  is the columnwise vector-to-matrix reshaping operator. Hence, the expected squared recovery error is proportional to the weighted sum of the squared frequency magnitude values in  $Y$ , where the weights are determined by the *error weighting factor*  $S_{R_{B,P}}$ . We derive an analytical expression for  $S_{R_{B,P}}$ , which makes use of the following lemma.

<sup>3</sup>The cross-correlations are linear in  $X$ , and hence such  $M_{R_B}$  and  $M_{R_P}$  exist for the noiseless cross-correlations  $C_{[X, R_B]}^\circ$  and  $C_{[X, R_P]}^\circ$ .

**Lemma 3.1** (Chapter 1 of [Str12]). *The singular value decomposition  $\mathbf{1}_L = U\Sigma V^T$  is such that for  $t, s \in \{0, \dots, n-1\}$ ,  $U$  and  $V$  have columns given by*

$$u_s(t) = \frac{1}{\sqrt{\frac{n}{2} + \frac{1}{4}}} \sin \left\{ \frac{(s + \frac{1}{2})(t + 1)}{n + \frac{1}{2}} \pi \right\},$$

$$v_s(t) = \frac{1}{\sqrt{\frac{n}{2} + \frac{1}{4}}} \cos \left\{ \frac{(s + \frac{1}{2})(t + \frac{1}{2})}{n + \frac{1}{2}} \pi \right\},$$

respectively, and  $\Sigma$  has diagonal entries given by

$$\sigma_s = \left[ 2 - 2 \cos \left( \frac{s + \frac{1}{2}}{n + \frac{1}{2}} \pi \right) \right]^{-1/2}.$$

**Proposition 3.2.** *For any  $k_1, k_2 \in \{0, \dots, m-1\}$ ,  $S_{R_{B,P}}(k_1, k_2)$  is equal to*

$$\frac{1}{m^4} \sum_{r,s=0}^{n-1} \left| \frac{\sigma_r \sigma_s}{\sigma_r^2 \sigma_s^2 + 1} u_r^\top (\mathcal{P}_2 F^*)(:, k_1) u_s^\top (\mathcal{P}_1 F^*)(:, k_2) + \frac{1}{\sigma_r^2 \sigma_s^2 + 1} v_r^\top (\mathcal{P}_1 F^*)(:, k_1) v_s^\top (\mathcal{P}_2 F^*)(:, k_2) \right|^2. \quad (3.5)$$

**Proof.** In the recovery algorithm,  $M = [\mathbf{1}_L \otimes \mathbf{1}_L; I_{n^2}]$ , so

$$\begin{aligned} M^\dagger &= [(\mathbf{1}_L^\top \otimes \mathbf{1}_L^\top) (\mathbf{1}_L \otimes \mathbf{1}_L) + I_{n^2}]^{-1} [\mathbf{1}_L^\top \otimes \mathbf{1}_L^\top, I_{n^2}] \\ &= [(\mathbf{1}_L^\top \mathbf{1}_L) \otimes (\mathbf{1}_L^\top \mathbf{1}_L) + I_{n^2}]^{-1} [\mathbf{1}_L^\top \otimes \mathbf{1}_L^\top, I_{n^2}], \end{aligned}$$

where we have used the mixed product property of Kronecker product. Write the SVD of  $\mathbf{1}_L$  as  $\mathbf{1}_L = U\Sigma V^\top$ . Using the spectral property of Kronecker product plus identity as contained in Eq. (5) of [SLM<sup>+</sup>11], we obtain

$$[(\mathbf{1}_L^\top \mathbf{1}_L) \otimes (\mathbf{1}_L^\top \mathbf{1}_L) + I_{n^2}]^{-1} = (V \otimes V) (\Sigma^2 \otimes \Sigma^2 + I_{n^2})^{-1} (V^\top \otimes V^\top).$$

Thus,

$$\begin{aligned} & [(\mathbf{1}_L^\top \mathbf{1}_L) \otimes (\mathbf{1}_L^\top \mathbf{1}_L) + I_{n^2}]^{-1} (\mathbf{1}_L^\top \otimes \mathbf{1}_L^\top) \\ &= (V \otimes V) (\Sigma^2 \otimes \Sigma^2 + I_{n^2})^{-1} (V^\top \otimes V^\top) (\mathbf{1}_L^\top \otimes \mathbf{1}_L^\top) \\ &= (V \otimes V) (\Sigma^2 \otimes \Sigma^2 + I_{n^2})^{-1} [(V^\top \mathbf{1}_L^\top) \otimes (V^\top \mathbf{1}_L^\top)] \\ &= (V \otimes V) (\Sigma^2 \otimes \Sigma^2 + I_{n^2})^{-1} [(\Sigma U^\top) \otimes (\Sigma U^\top)] \\ &= (V \otimes V) (\Sigma^2 \otimes \Sigma^2 + I_{n^2})^{-1} (\Sigma \otimes \Sigma) (U^\top \otimes U^\top) \\ &= (V \otimes V) [(\Sigma^2 \otimes \Sigma^2 + I_{n^2})^{-1} (\Sigma \otimes \Sigma)] (U^\top \otimes U^\top). \end{aligned}$$

Combining the partial results above, we obtain

$$\begin{aligned} T_R &= \frac{1}{m^2} (V \otimes V) \left[ (\Sigma^2 \otimes \Sigma^2 + I_{n^2})^{-1} (\Sigma \otimes \Sigma) (U^\top \otimes U^\top) (\mathcal{P}_2 F^* \otimes \mathcal{P}_1 F^*) \right. \\ &\quad \left. + (\Sigma^2 \otimes \Sigma^2 + I_{n^2})^{-1} (V^\top \otimes V^\top) (\mathcal{P}_1 F^* \otimes \mathcal{P}_2 F^*) \right] \\ &= \frac{1}{m^2} (V \otimes V) \left[ (\Sigma^2 \otimes \Sigma^2 + I_{n^2})^{-1} (\Sigma \otimes \Sigma) (U^\top \mathcal{P}_2 F^* \otimes U^\top \mathcal{P}_1 F^*) \right. \\ &\quad \left. + (\Sigma^2 \otimes \Sigma^2 + I_{n^2})^{-1} (V^\top \mathcal{P}_1 F^* \otimes V^\top \mathcal{P}_2 F^*) \right]. \end{aligned}$$

From Eq. (3.4), it follows that  $S_{R_{B,P}}(k_1, k_2) = \|T'_R(:, mk_1 + k_2)\|^2$  and thus we are interested in the squared column norms of  $T_R$ . Since  $V \otimes V$  is an orthogonal matrix and the Euclidean norm is orthogonally invariant, it is enough to consider the squared column norms of

$$T'_R = \frac{1}{m^2} \left[ (\Sigma^2 \otimes \Sigma^2 + I_{n^2})^{-1} (\Sigma \otimes \Sigma) (U^\top \mathcal{P}_2 F^* \otimes U^\top \mathcal{P}_1 F^*) + (\Sigma^2 \otimes \Sigma^2 + I_{n^2})^{-1} (V^\top \mathcal{P}_1 F^* \otimes V^\top \mathcal{P}_2 F^*) \right].$$

For any  $(k_1, k_2) \in \{0, 1, \dots, m-1\} \times \{0, 1, \dots, m-1\}$  and the corresponding  $k = mk_1 + k_2$ ,

$$\begin{aligned} & \|T'_R(:, k)\|^2 \\ &= \frac{1}{m^4} \sum_{r,s=0}^{n-1} \left| \frac{\sigma_r \sigma_s}{\sigma_r^2 \sigma_s^2 + 1} [U^\top \mathcal{P}_2 F^*](r, k_1) [U^\top \mathcal{P}_1 F^*](s, k_2) + \frac{1}{\sigma_r^2 \sigma_s^2 + 1} [V^\top \mathcal{P}_1 F^*](r, k_1) [V^\top \mathcal{P}_2 F^*](s, k_2) \right|^2 \\ &= \frac{1}{m^4} \sum_{r,s=0}^{n-1} \left| \frac{\sigma_r \sigma_s}{\sigma_r^2 \sigma_s^2 + 1} u_r^\top (\mathcal{P}_2 F^*)(:, k_1) u_s^\top (\mathcal{P}_1 F^*)(:, k_2) + \frac{1}{\sigma_r^2 \sigma_s^2 + 1} v_r^\top (\mathcal{P}_1 F^*)(:, k_1) v_s^\top (\mathcal{P}_2 F^*)(:, k_2) \right|^2, \end{aligned}$$

as claimed. ■

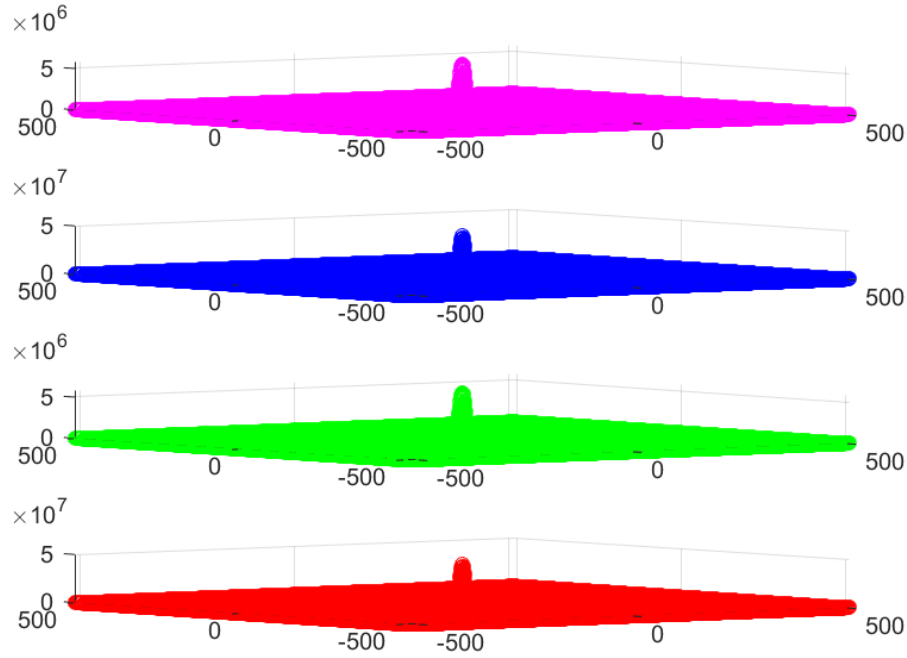


**Figure 5:** Top to bottom: squared magnitudes of the Fourier transform of the mimivirus [GKL<sup>+</sup>08] itself, and that of combined with the block, pinhole, and dual-references, respectively (with  $n = 64$ , and  $m = 1024$ ). These four spectra exhibit similar low-frequency dominance, and have entries of similar orders of magnitude.

In the expected squared recovery error Eq. (3.3), both  $Y$  and  $S_R$  depend on the reference scheme in use. Empirically, for low-frequency dominant  $X$  with typical  $[0, 1]$  values (e.g., images shown in Fig. 2 and Fig. 7, typical CDI specimens),  $Y$  will have a similar spectrum to  $X$  (up to small variation in the order of magnitude) for the various reference schemes of interest; see Fig. 5. This stability property of spectrum can be formally established for the single-reference setup  $[X, R]$  by expanding  $|\widehat{[X, R]}|^2$  [BSC<sup>+</sup>19], and likewise for

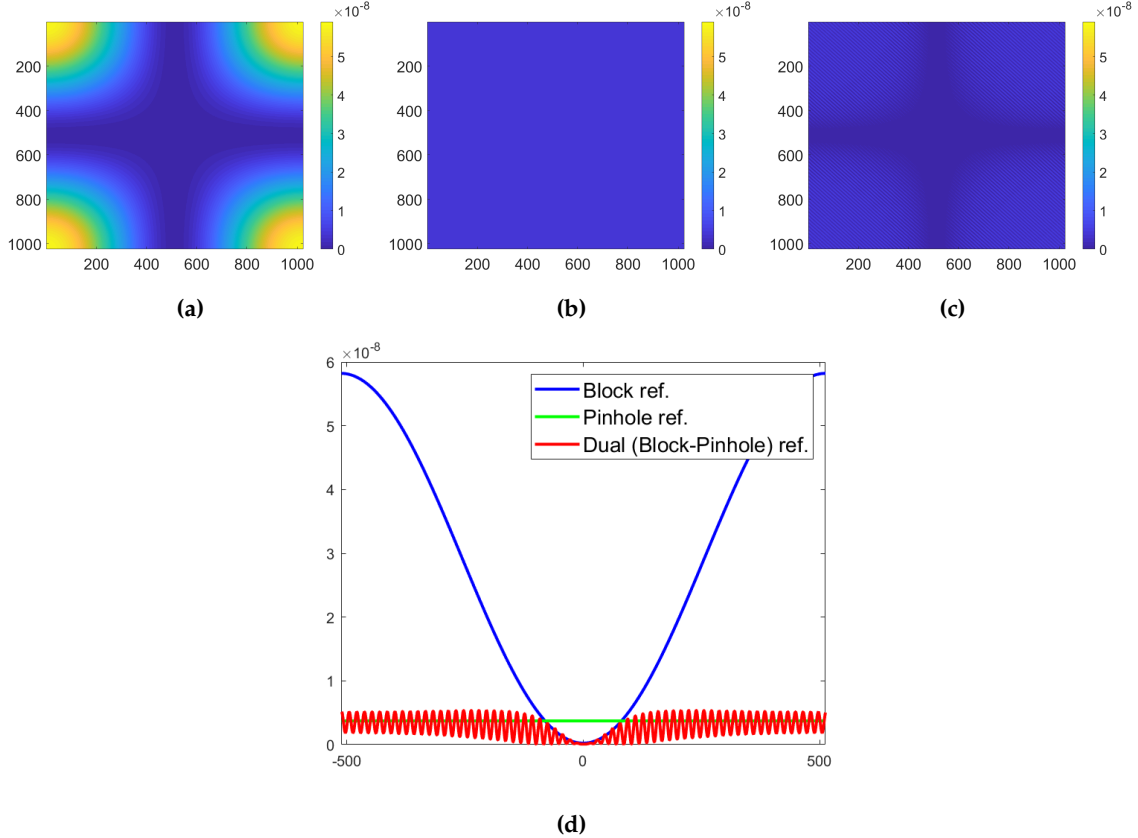


**Figure 6:** The top row shows colormap plots of the weighting factors  $S_R$  for the block, pinhole, and dual references, respectively, when  $n = 64$  and  $m = 1024$ . The bottom plot shows the three weighting factors along the (four identical) bordering cross-sections of the colormap plots.

our dual-reference setup  $\mathcal{X}$ . In contrast, the weighting factors in  $S_R$  can vary by several orders of magnitudes for different reference schemes, as shown in Fig. 6. Hence, the influence of the reference scheme on the expected squared error is largely determined by  $S_R$ .

In Fig. 6, we compare the  $S_R$ 's for the single-reference setup with the pinhole and block references, with that of our dual-reference setup. For the single-reference setup  $[X, R]$ , [BSC<sup>+</sup>19] showed that among all reference choices, the block and pinhole references put minimal error weighting for low- and high-frequency components of  $Y$ , respectively. The strikingly simple idea of including the two references simultaneously and solving the resulting stacked linear system helps to combine the benefits: as can be seen from Fig. 6,  $S_{R_{B,P}}$  approximates the smaller of  $S_{R_B}$  and  $S_{R_P}$  uniformly over the entire frequency spectrum.

## 4 Numerical Simulations

We observe in numerical simulation of CDI experiments that the dual-reference provides smaller recovery error than does the leading single-reference schemes, specifically the block and pinhole references. A data comparison is provided in Table 1 for a variety of macromolecular, cellular, and crystalline specimens, such as those studied using CDI. These include the mimivirus image [GKL<sup>+</sup>08] shown in Fig. 2 and Fig. 4 and the images shown in Fig. 7.



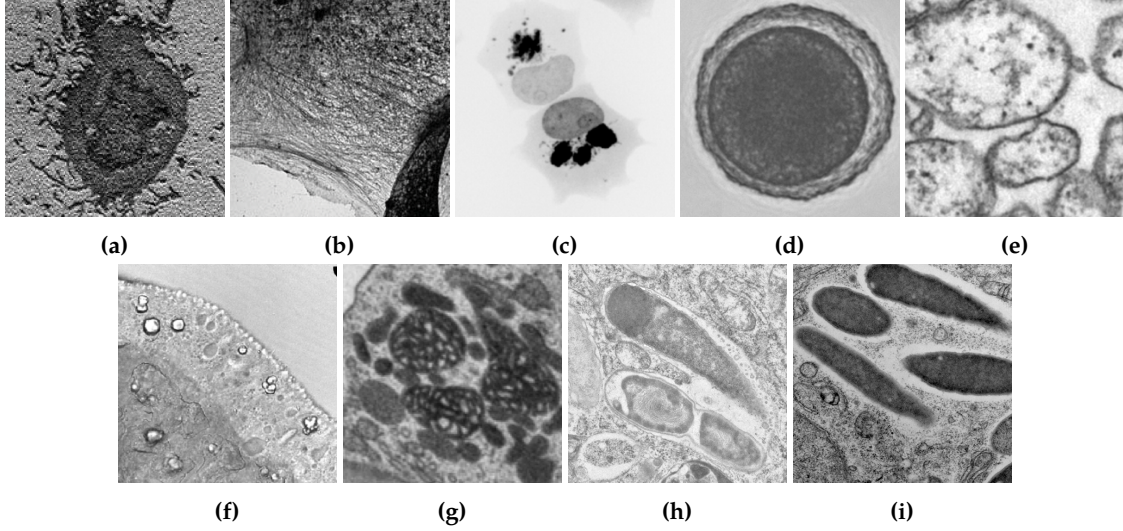


**Figure 7:** CDI specimen images used for numerical simulations in Table 1. Shown are specimens of influenza virus [KDS<sup>+</sup>15], stroma cells [KDS<sup>+</sup>15], mCherry proteins [PNE16], 2-cell embryo [EGH<sup>+</sup>11], oocytes [EGH<sup>+</sup>11], *S. pistillata* [VTH<sup>+</sup>11], in-cellular aragonite crystal [MSH<sup>+</sup>18], salmonella WT [RLC<sup>+</sup>14], and sifA salmonella strain [RLC<sup>+</sup>14], respectively.

**Table 1:** Empirical and expected values (shown in brackets) for the relative squared errors  $\|X^* - X\|_F^2 / \|X\|_F^2$ . The error values are the reported values rescaled by  $10^{-4}$ . Test images  $X$  of size  $64 \times 64$  pixels are the mimivirus shown in Fig. 2, and the images shown in Fig. 7. Simulated photon flux data is of size  $1024 \times 1024$ , with  $N_p = 1000(1024^2)$  (i.e. 1000 photons per pixel).

Image	Block Ref.	Pinhole Ref.	Dual Ref.	HIO (No Ref.)
Mimivirus	3.7029 (3.7953)	46.966 (63.835)	1.5155 (1.4525)	93.794
Influenza	18.7572 (18.5520)	50.719 (31.452)	4.6401 (4.7004)	695.73
Stroma cells	9.1943 (8.9122)	23.115 (44.197)	2.7841 (2.6360)	1607.0
mCherry proteins	1.8461 (1.8458)	139.50 (131.54)	0.9279 (0.9086)	403.13
Embryo	6.3037 (6.2949)	54.205 (53.824)	2.6294 (2.7130)	642.46
Oocytes	7.0095 (6.8380)	44.184 (78.367)	2.6675 (2.7010)	883.06
<i>S. pistillata</i>	4.0266 (3.9307)	148.83 (83.753)	1.2935 (1.3175)	335.69
Aragonite	11.619 (11.542)	52.103 (34.657)	4.4102 (4.4102)	1767.3
Salmonella WT	9.0773 (8.8195)	44.392 (60.197)	3.3348 (2.9799)	708.05
sifA	7.2709 (7.1516)	42.625 (54.657)	2.8244 (2.8651)	1765.6

## 5 Conclusions

We have proposed a new dual-reference scheme for Holographic CDI, together with a recovery algorithm which provides exact recovery in the noiseless setting. For data following a Poisson shot noise distribution, the dual-reference gives an expected recovery error which minimizes the weighting of error across the frequency spectrum, effectively combining the best features of both the individual block and pinhole references. Numerical experiments on simulated CDI data show the dual-reference scheme provides a smaller recovery error than the leading (single) reference schemes.



## Acknowledgements

The authors are very grateful to Walter Murray and Gordon Wetzstein for many guiding discussions throughout this research.

## References

- [BSC<sup>+</sup>19] David A. Barmherzig, Ju Sun, Emmanuel J. Candes, T. J. Lane, and Po-Nan Li, *Holographic Phase Retrieval and Optimal Reference Design*, arXiv e-prints (2019), arXiv:1901.06453.
- [EGH<sup>+</sup>11] Michael Eitel, Loretta Guidi, Heike Hadrys, Maria Balsamo, and Bernd Schierwater, *New insights into placozoan sexual reproduction and development*, PLOS ONE **6** (2011), no. 5, 1–9.
- [GKL<sup>+</sup>08] Eric Ghigo, Jürgen Kartenbeck, Pham Lien, Lucas Pelkmans, Christian Capo, Jean-Louis Mege, and Didier Raoult, *Ameobal Pathogen Mimivirus Infects Macrophages through Phagocytosis*, PLOS Pathogens **4** (2008), no. 6, 1–17.
- [KDS<sup>+</sup>15] Doory Kim, Thomas J. Deerinck, Yaron M. Sigal, Hazen P. Babcock, Mark H. Ellisman, and Xiaowei Zhuang, *Correlative stochastic optical reconstruction microscopy and electron microscopy*, PLOS ONE **10** (2015), no. 4, 1–20.
- [MCKS99] Jianwei Miao, Pambos Charalambous, Janos Kirz, and David Sayre, *Extending the methodology of X-ray crystallography to allow imaging of micrometre-sized non-crystalline specimens*, Nature **400** (1999), 342–344.
- [MSH<sup>+</sup>18] Tatiana D. Mayorova, Carolyn L. Smith, Katherine Hammar, Christine A. Winters, Natalia B. Pivovarova, Maria A. Aronova, Richard D. Leapman, and Thomas S. Reese, *Cells containing aragonite crystals mediate responses to gravity in trichoplax adhaerens (placozoa), an animal lacking neurons and synapses*, PLOS ONE **13** (2018), no. 1, 1–20.
- [OS09] Alan V. Oppenheim and Ronald W. Schaffer, *Discrete-time signal processing*, 3rd ed., Prentice Hall Press, Upper Saddle River, NJ, USA, 2009.
- [PNE16] Patrick Paszkowski, Ryan S. Noyce, and David H. Evans, *Live-cell imaging of vaccinia virus recombination*, PLOS Pathogens **12** (2016), no. 8, 1–28.
- [RLC<sup>+</sup>14] Roopa Rajashekar, David Liebl, Deepak Chikkaballi, Viktoria Liss, and Michael Hensel, *Live cell imaging reveals novel functions of salmonella enterica spi2-t3ss effector proteins in remodeling of the host cell endosomal system*, PLOS ONE **9** (2014), no. 12, 1–29.
- [SLLF12] M Saliba, T Latychevskaia, J Longchamp, and H Fink, *Fourier Transform Holography: A Lensless Non-Destructive Imaging Technique*, Microscopy and Microanalysis **18** (2012), no. S2, 564–565.
- [SLM<sup>+</sup>11] Oliver Stegle, Christoph Lippert, Joris M Mooij, Neil D Lawrence, and Karsten M Borgwardt, *Efficient inference in matrix-variate gaussian models with iid observation noise*, Advances in neural information processing systems, 2011, pp. 630–638.
- [Str12] Gilbert Strang, *Computational science and engineering*, Wellesley-Cambridge Press, Wellesley, MA, USA, 2012.
- [VTH<sup>+</sup>11] Alexander Venn, Eric Tambutt-Äl, Michael Holcomb, Denis Allemand, and Sylvie Tambutt-Äl, *Live tissue imaging shows reef corals elevate ph under their calcifying tissue relative to seawater*, PLOS ONE **6** (2011), no. 5, 1–9.
- [WTT<sup>+</sup>16] I S Wahyutama, G K Tadesse, A Tünnermann, J Limpert, and J Rothhardt, *Influence of detector noise in holographic imaging with limited photon flux*, Opt. Express **24** (2016), no. 19, 22013–22027.